Electronic Supplementary Material (ESI) for Chemical Communications
This journal is © The Royal Society of Chemistry 2011

Spin-selective recombination kinetics of a model chemical magnetoreceptor

Supporting Information

K. Maeda[1,2], C. J. Wedge[1,&], J. G Storey[1], K. B Henbest[1,2], P. A. Liddell[3], G. Kodis[3], D. Gust[3], P. J. Hore[2] and C. R. Timmel[1].

[1]Department of Chemistry, University of Oxford,
Centre for Advanced Electron Spin Resonance and Inorganic Chemistry Laboratory,
Oxford, OX1 3QR, UK

[2]Department of Chemistry, University of Oxford,
Physical and Theoretical Chemistry Laboratory, Oxford, OX1 3QZ, UK

[3]Department of Chemistry and Biochemistry, Arizona State University, Tempe,
Arizona 85287, USA.

[&]Current address: Department of Physics, University of Oxford,
Clarendon Laboratory, Oxford, OX1 3PU

Contents

1. Magnetic field effect (MFE) data
2. Reaction yield detected magnetic resonance (RYDMR) data
3. Time-resolved continuous wave EPR
4. Pulsed EPR
5. Simulation of MFE data
6. Simulation of RYDMR data

1. Magnetic field effect (MFE) data

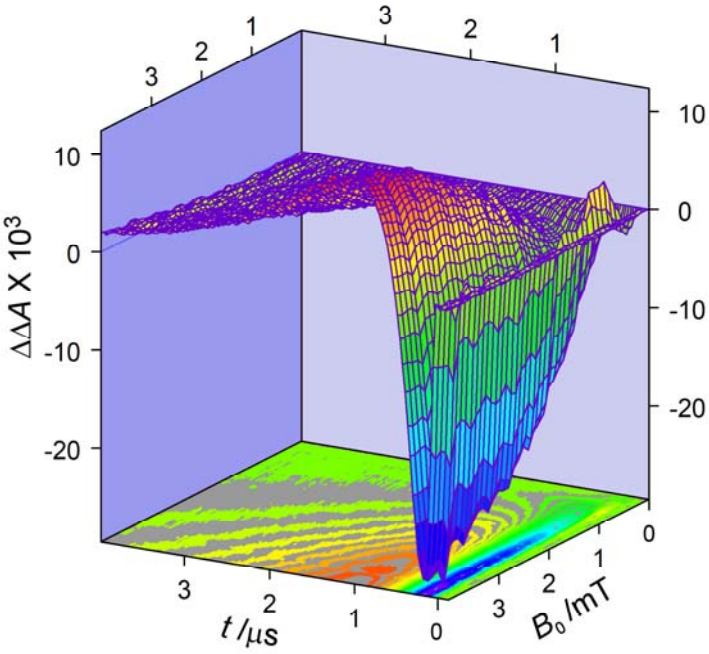

Figure S1. Time-resolved static magnetic field effect on the recombination of $C^{\bullet+}PF^{\bullet-}$. $\Delta\Delta A$ is the difference in the transient absorption signal of $F^{\bullet-}$ with and without the static magnetic field B_0. Note that the signal changes sign at a time ~300 ns after the laser flash.

2. Reaction yield detected magnetic resonance (RYDMR) data

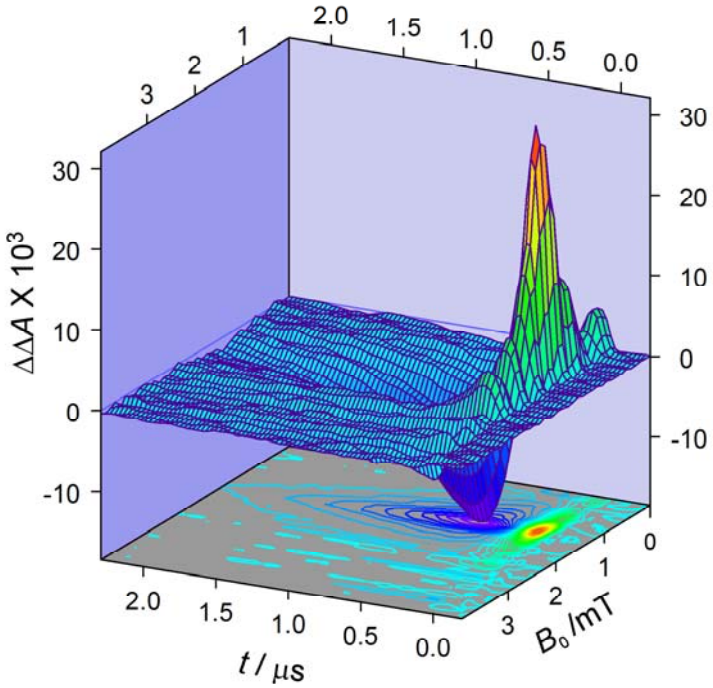

Figure S2. Time-resolved radiofrequency magnetic field effect on the recombination of $C^{\bullet+}PF^{\bullet-}$. $\Delta\Delta A$ is the difference in the transient absorption signal of $F^{\bullet-}$ with and without a 0.14 mT, 36 MHz radiofrequency field in the presence of a static magnetic field B_0. Note that the signal changes sign at a time ~300 ns after the laser flash.

3. Time-resolved continuous wave EPR

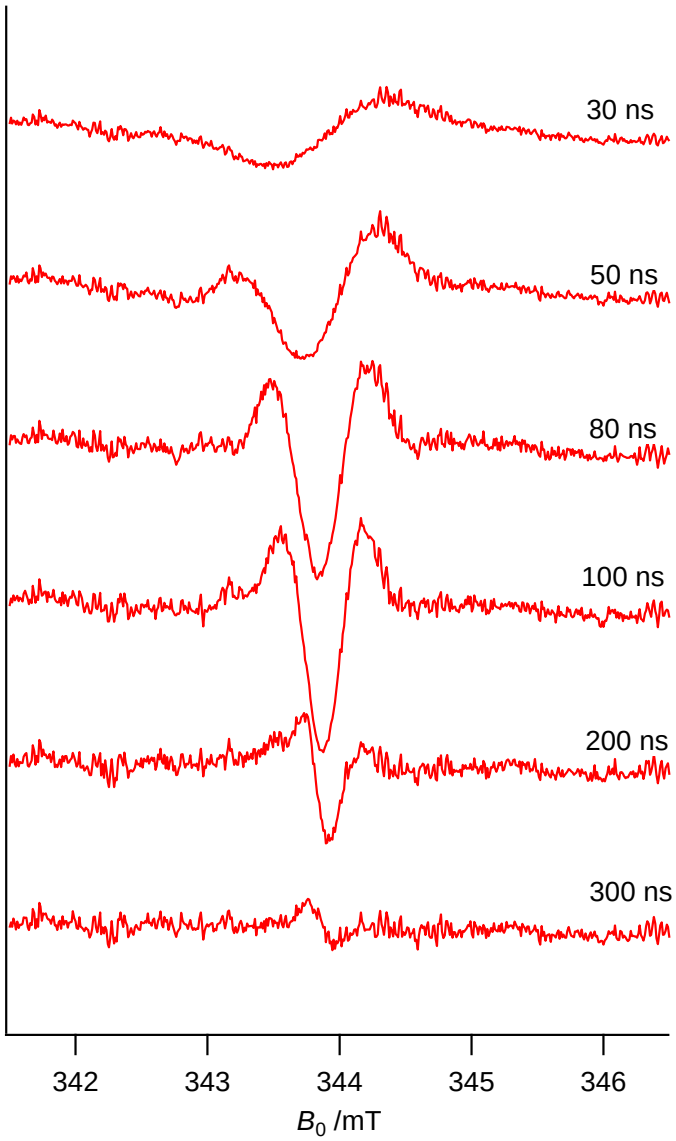

Figure S3. Time-resolved X-band EPR spectra of $C^{\bullet+}PF^{\bullet-}$ in MTHF solution at 119 K. The boxcar window for signal averaging was 20 ns for $30\ \text{ns} < t < 100\ \text{ns}$ and 50 ns for $t = 200$ ns and 300 ns. The phase inversion from an initial EA pattern (emission at low field, absorption at high field) to an AE pattern at later times can clearly be seen. As usual in such spectra, the EPR lines are broadened at the earliest times.

4. Pulsed EPR

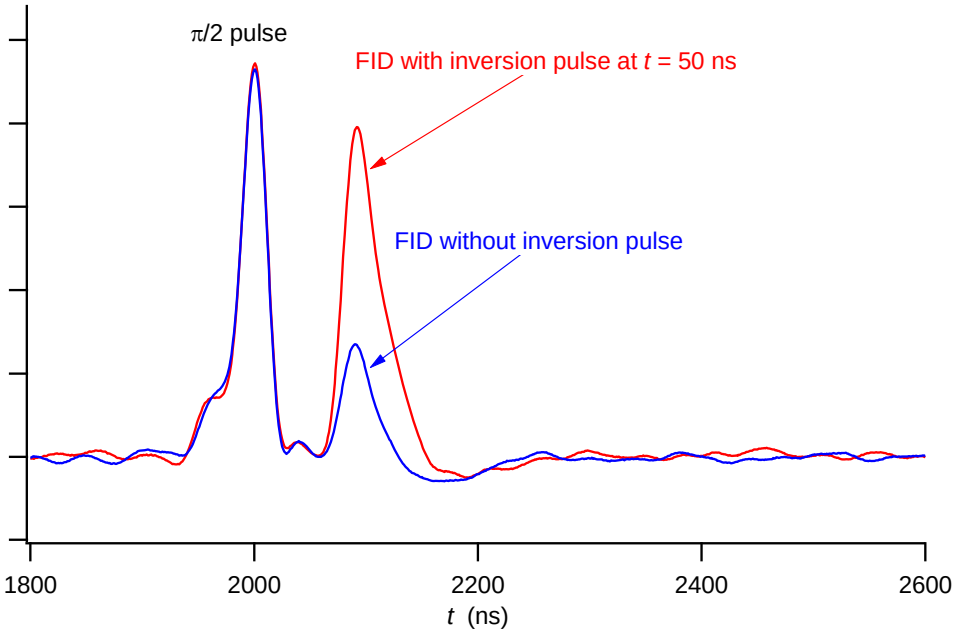

Figure S4. X-band EPR FID (free induction decay) signal of $C^{\bullet+}PF^{\bullet-}$ following a π/2-pulse (16 ns duration) at time $\tau_1 + \tau_2 = 2$ μs after laser excitation (see Figure 2A for pulse sequence timings). The red and blue traces were recorded under identical conditions except that the π-pulse (32 ns duration) at $\tau_1 = 50$ ns was not present in the latter. The boost in the FID intensity caused by the π-pulse provides direct evidence that the back electron transfer reaction from the singlet state of the radical pair is faster than that from the triplet state ($k_S > k_T$). The EPR spectrum of $C^{\bullet+}$ is too broad to make a significant contribution to the detected signal, so that the FID is dominated by $F^{\bullet-}$.

The time-dependence in Figure 2A can be understood as follows:

- Assume $k_S\tau_2 >> 1$ and $k_T\tau_1,\ k_T\tau_2 << 1$.
- Treat the M_a and M_b states together as level 1, and the $T_{\pm1}$ states together as level 2.
- As M_a and M_b are 50% singlet and 50% triplet, and because we assume $k_S >> k_T$, the radical pairs in level 1 recombine at a rate $\frac{1}{2}k_S$. As level 2 is 100% triplet, its population recombines at a rate k_T.
- Take the initial populations to be $n_1(0) = 1 - \frac{2}{3}\lambda$ and $n_2(0) = \frac{2}{3}\lambda$ where λ is small (see main text).

Just before the π-pulse at time τ_1:

$$\begin{aligned} n_1(\tau_1) &= n_1(0)\mathrm{e}^{-\frac{1}{2}k_S\tau_1} \\ n_2(\tau_1) &= n_2(0) \end{aligned} \tag{S1}$$

The π-pulse swaps over the populations of levels 1 and 2, so that just after π-pulse:

$$\begin{aligned} n_1(\tau_1) &= n_2(0) \\ n_2(\tau_1) &= n_1(0)\mathrm{e}^{-\frac{1}{2}k_S\tau_1} \end{aligned} \tag{S2}$$

After a further time τ_2:

$$\begin{aligned} n_1(\tau_1,\tau_2) &= n_2(0)\mathrm{e}^{-\frac{1}{2}k_S\tau_2} \approx 0 \\ n_2(\tau_1,\tau_2) &= n_1(0)\mathrm{e}^{-\frac{1}{2}k_S\tau_1} = (1-\tfrac{2}{3}\lambda)\mathrm{e}^{-\frac{1}{2}k_S\tau_1} \end{aligned} \tag{S3}$$

The EPR signal is then

$$\begin{aligned} I(\tau_1,\tau_2) &= n_2(\tau_1,\tau_2) - n_1(\tau_1,\tau_2) \\ &= (1-\tfrac{2}{3}\lambda)\mathrm{e}^{-\frac{1}{2}k_S\tau_1} \end{aligned} \tag{S4}$$

When the pulse sequence is repeated without a π-pulse:

$$\begin{aligned} n_1'(\tau_1,\tau_2) &= n_1(0)\mathrm{e}^{-\frac{1}{2}k_S(\tau_1+\tau_2)} \approx 0 \\ n_2'(\tau_1,\tau_2) &= n_2(0) = \tfrac{2}{3}\lambda \\ I'(\tau_1,\tau_2) &= n_2'(\tau_1,\tau_2) - n_1'(\tau_1,\tau_2) \\ &= \tfrac{2}{3}\lambda \end{aligned} \tag{S5}$$

Therefore the difference signal displayed in Figure 2A is:

$$I(\tau_1,\tau_2) - I'(\tau_1,\tau_2) = (1-\tfrac{2}{3}\lambda)\mathrm{e}^{-\frac{1}{2}k_S\tau_1} - \tfrac{2}{3}\lambda \tag{S6}$$

The data in Figure 2A give $k_S \approx 1.8 \times 10^7\ \mathrm{s}^{-1}$ and $\lambda \approx 0.07$.

5. Simulation of MFE data

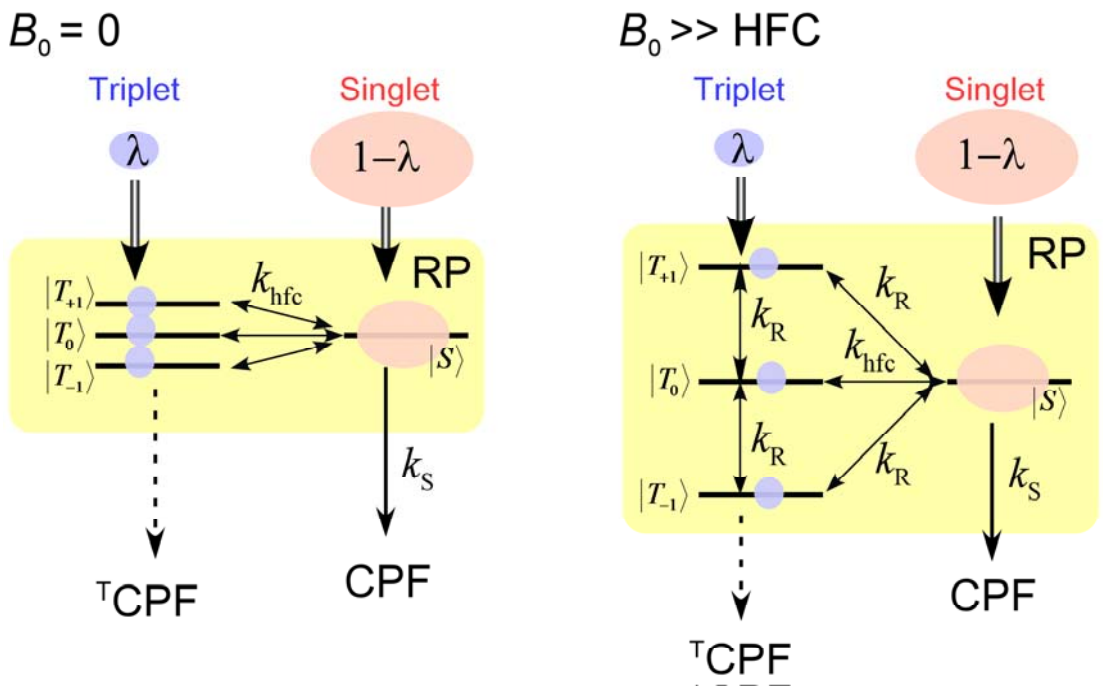

Figure S5. Schematic of the model used to simulate magnetic field effects on the recombination kinetics of $C^{\bullet+}PF^{\bullet-}$.

Analysis of the MFE time profiles was performed using the kinetic model[1,2] shown in Figure S5. The radical pair has four electronic spin states, however when the exchange interaction of the two radicals is small, T_0 and S are degenerate and we can reduce the model to two composite states, M and T, with populations:

$$[\mathrm{T}] = [\mathrm{T}_{+1}] + [\mathrm{T}_{-1}]; \qquad [\mathrm{M}] = [\mathrm{S}] + [\mathrm{T}_0] \tag{S7}$$

When the frequency of S ↔ T interconversion as a result of hyperfine interactions k_{hfc} is much larger than both the spin relaxation rate k_R and the recombination rates k_S and k_T, and when the applied magnetic field B_0 is much stronger than the hyperfine interactions, we have:

$$\begin{aligned} \frac{\mathrm{d}[\mathrm{T}]}{\mathrm{d}t} &= -k_R[\mathrm{T}] + k_R[\mathrm{M}] \\ \frac{\mathrm{d}[\mathrm{M}]}{\mathrm{d}t} &= k_R[\mathrm{T}] - (k_R + \tfrac{1}{2}k_S)[\mathrm{M}] \end{aligned} \tag{S8}$$

and when $B_0 = 0$

$$\begin{aligned} \frac{\mathrm{d}[\mathrm{T}]}{\mathrm{d}t} &= -k_{\mathrm{hfc}}[\mathrm{T}] + k_{\mathrm{hfc}}[\mathrm{M}] \\ \frac{\mathrm{d}[\mathrm{M}]}{\mathrm{d}t} &= k_{\mathrm{hfc}}[\mathrm{T}] - \left(k_{\mathrm{hfc}} + \tfrac{1}{2}k_{\mathrm{S}}\right)[\mathrm{M}] \end{aligned} \tag{S9}$$

The transient absorption signal $\Delta A(B_0,t)$ can be calculated as

$$\Delta A(B_0,t) \propto [\mathrm{M}] + [\mathrm{T}] \tag{S10}$$

We consider the case of an initial mixture of S and T radical pairs, with the triplet population distributed evenly amongst the three triplet sublevels. Denoting the initial triplet fraction λ, we have

$$\begin{aligned} [\mathrm{T}]_0 &= \frac{2}{3}\lambda \\ [\mathrm{M}]_0 &= \frac{1}{3}\lambda + (1-\lambda) = 1 - \frac{2}{3}\lambda \end{aligned} \tag{S11}$$

Equations (S8)-(S11) were solved numerically to obtain the time evolution of $\Delta A(B_0,t)$ and $\Delta A(0,t)$, from which the MFE time-profile may be calculated as

$$\Delta\Delta A(B_0,t) \propto \Delta A(B_0,t) - \Delta A(0,t) \tag{S12}$$

To fit the data shown in Figure 2B, we used $k_{\mathrm{S}} = 1.8 \times 10^7\ \mathrm{s}^{-1}$ (obtained from the EPR time-dependence in Figure 2A, see above) and $k_{\mathrm{hfc}} \approx 1 \times 10^8\ \mathrm{s}^{-1}$, a reasonable value given the hyperfine coupling constants of the carotenoid radical; the simulations were not particularly sensitive to this parameter. In the fitting, we optimized only k_{R} for various values of λ, with the following results:

λ	Optimized relaxation rate at 4 mT k_R / 10^6 s^{-1}
0.00	0.71
0.04	0.42
0.07	0.35
0.10	0.35

The best fit to the data in Figure 2B was obtained with $\lambda = 0.07$.

The form of the time-dependence of the data in Figure 2B can be understood using a simple analytical treatment. Taking $\lambda = 0$ for simplicity, Equation (S8) gives the following expression for the total amount of radical pair in the presence of the magnetic field:

$$\begin{aligned}[\mathrm{M}]_\mathrm{B} + [\mathrm{T}]_\mathrm{B} &= \exp\left[-(k_\mathrm{R} + k_\mathrm{S}/4 + \Omega_\mathrm{B}/4)t\right]\left(\tfrac{1}{2} - X_\mathrm{B}\right) \\ &\quad + \exp\left[-(k_\mathrm{R} + k_\mathrm{S}/4 - \Omega_\mathrm{B}/4)t\right]\left(\tfrac{1}{2} + X_\mathrm{B}\right)\end{aligned} \tag{S13}$$

where

$$\Omega_\mathrm{B} = \sqrt{16k_\mathrm{R}^2 + k_\mathrm{S}^2}; \qquad X_\mathrm{B} = \frac{4k_\mathrm{R} - k_\mathrm{S}}{2\Omega_\mathrm{B}} \tag{S14}$$

Similarly, at zero field, Equation (S9) gives

$$\begin{aligned}[\mathrm{M}]_0 + [\mathrm{T}]_0 &= \exp\left[-(k_\mathrm{HFC} + k_\mathrm{S}/4 + \Omega_0/4)t\right]\left(\tfrac{1}{2} - X_0\right) \\ &\quad + \exp\left[-(k_\mathrm{HFC} + k_\mathrm{S}/4 - \Omega_0/4)t\right]\left(\tfrac{1}{2} + X_0\right)\end{aligned} \tag{S15}$$

with

$$\Omega_0 = \sqrt{16k_\mathrm{HFC}^2 + k_\mathrm{S}^2}; \qquad X_0 = \frac{4k_\mathrm{HFC} - k_\mathrm{S}}{2\Omega_\mathrm{B}} \tag{S16}$$

In the limiting case $k_\mathrm{HFC} >> k_\mathrm{S} >> k_\mathrm{R}$, Equations (S15) and (S16) become, respectively

$$[\mathrm{M}]_{\mathrm{B}} + [\mathrm{T}]_{\mathrm{B}} \approx \mathrm{e}^{-\frac{1}{2}k_{\mathrm{S}}t} + \frac{2k_{\mathrm{R}}}{k_{\mathrm{S}}}\left[\mathrm{e}^{-k_{\mathrm{R}}t} - \mathrm{e}^{-\frac{1}{2}k_{\mathrm{S}}t}\right] \tag{S17}$$

and

$$[\mathrm{M}]_{0} + [\mathrm{T}]_{0} \approx \mathrm{e}^{-\frac{1}{4}k_{\mathrm{S}}t} \tag{S18}$$

Although the data in Figure 2B are not strictly in the $k_{\mathrm{HFC}} >> k_{\mathrm{S}} >> k_{\mathrm{R}}$ limit, Equations (S17) and (S18) nevertheless account for the general form of the time-dependence of the field-on minus field-off signal $[\mathrm{M}]_{\mathrm{B}} + [\mathrm{T}]_{\mathrm{B}} - [\mathrm{M}]_{0} - [\mathrm{T}]_{0}$, i.e. a rapid rise with a somewhat slower fall superimposed on a much slower and weaker decay of opposite phase.

6. Simulation of RYDMR data

Simulation of the RYDMR data in Figure 2C was performed using a brute-force Liouville space approach, working in the laboratory frame throughout. The equation of motion for the state of the system is the Liouville–von Neumann equation:

$$\frac{\mathrm{d}\left|\rho(t)\right\rangle}{\mathrm{d}t} = \left(-\mathrm{i}\hat{\hat{H}}^{\times}(t) + \hat{\hat{K}} + \hat{\hat{R}}\right)\left|\rho(t)\right\rangle \tag{S19}$$

Here, $\left|\rho(t)\right\rangle$ is the spin density operator, $\hat{\hat{H}}^{\times}(t)$ is the spin Hamiltonian commutation superoperator, $\hat{\hat{K}}$ is the recombination kinetics superoperator and $\hat{\hat{R}}$ is the relaxation superoperator. We examine the various terms in this equation in detail below.

Hamiltonian

The simulated spin system consists of two electrons (1, 2), and two spin-½ nuclei (3, 4). Electron 1 has hyperfine interactions with both nuclei; electron 2 has no hyperfine coupling. This is an approximation of the CPF triad molecule, which consists of a carotenoid part with substantial hyperfine couplings, and a C_{60} part with minimal hyperfine couplings. The time-independent part of the spin Hamiltonian is

$$\hat{H}_0 = \left(g_1\hat{S}_{1,z} + g_2\hat{S}_{2,z}\right)\mu_{\mathrm{B}}B_0 + A_3\hat{S}_1\cdot\hat{I}_3 + A_4\hat{S}_1\cdot\hat{I}_4 \tag{S20}$$

where g_1 and g_2 are the g-values of the two radicals, and A_3 and A_4 are the two hyperfine coupling constants. The time-dependent part of the Hamiltonian represents the interaction of the spins with the oscillating (B_1) magnetic field:

$$\hat{H}_1(t) = \left(g_1\hat{S}_{1,x} + g_2\hat{S}_{2,x}\right)\mu_B B_1 \sin\left(\omega_{RF}t + \phi\right) \tag{S21}$$

where ω_{RF} is the frequency and ϕ is the phase of the radiofrequency field and B_1 is the peak RF field strength.

Recombination Superoperator

The recombination superoperator, $\hat{\hat{K}}$, follows the conventional Haberkorn model[3]:

$$\hat{\hat{K}}|\rho\rangle \Rightarrow -\frac{k_S}{2}\left(\hat{P}_S\hat{\rho} + \hat{\rho}\hat{P}_S\right) \tag{S22}$$

where we assume that recombination only occurs from the singlet state.

Relaxation Superoperator

The interaction of the two electron spins in $C^{\bullet+}PF^{\bullet-}$ is very weak so that we need not consider concerted relaxation processes. The spin relaxation superoperator can therefore be written as the sum of relaxation operators for the individual electrons:

$$\hat{\hat{R}} = \hat{\hat{R}}_1 + \hat{\hat{R}}_2 \tag{S23}$$

where nuclear spin relaxation is neglected. Each electron spin has longitudinal (T_1) and transverse (T_2) relaxation as follows:

$$\hat{\hat{R}}_i = -\frac{1}{T_{1,i}}\hat{\hat{R}}_{i,z} - \frac{1}{T_{2,i}}\left(\hat{\hat{R}}_{i,x} + \hat{\hat{R}}_{i,y}\right) \tag{S24}$$

The relaxation superoperators are constructed such that the $\hat{S}_{i,z}$ states of a given spin, i (= 1 or 2), relax at a rate $T_{1,i}^{-1}$, while the $\hat{S}_{i,x}$ and $\hat{S}_{i,y}$ states relax at a rate $T_{2,i}^{-1}$. Products of these states relax at a rate equal to the sum of the corresponding relaxation rates. For example, $\hat{S}_{1,z}\hat{S}_{2,x}$ would relax at a rate $T_{1,1}^{-1} + T_{2,2}^{-1}$.

We define the basis product operators[4]

$$\hat{B}(q,s) = 2^{\left[-1+\sum_{n=1}^{4} q_n\right]} \left(\hat{S}_{1,s_1}\right)^{q_1} \left(\hat{S}_{2,s_2}\right)^{q_2} \left(\hat{I}_{3,s_3}\right)^{q_3} \left(\hat{I}_{4,s_4}\right)^{q_4} \tag{S25}$$

where, $q_n = \{0,1\}$, and $s_n = \{x,y,z\}$ if $q_n = 1$, and $\hat{E}$ (the identity operator) if $q_n = 0$. The relaxation superoperators in Equation (S24) are:

$$\hat{\hat{R}}_{i,v} = \sum_{\substack{q_i=1;q_{n\neq i}=\{0,1\} \\ s_i=v;s_{n\neq i}=\begin{cases}\{x,y,z\} & \text{if } q_n=1 \\ \{e\} & \text{if } q_n=0\end{cases}}} \left|\hat{B}(q,s)\right\rangle\left\langle\hat{B}(q,s)\right| \tag{S26}$$

For example:

$$\begin{aligned}
\hat{\hat{R}}_{1,x} &= \left|S_{1x}\right\rangle\left\langle S_{1x}\right| \\
&+ \sum_{\mu=x,y,z} \left[\left|2S_{1x}S_{2\mu}\right\rangle\left\langle 2S_{1x}S_{2\mu}\right| + \left|2S_{1x}I_{3\mu}\right\rangle\left\langle 2S_{1x}I_{3\mu}\right| + \left|2S_{1x}I_{4\mu}\right\rangle\left\langle 2S_{1x}I_{4\mu}\right|\right] \\
&+ \sum_{\mu,\nu=x,y,z} \left[\left|4S_{1x}S_{2\mu}I_{3\nu}\right\rangle\left\langle 4S_{1x}S_{2\mu}I_{3\nu}\right| + \left|4S_{1x}S_{2\mu}I_{4\nu}\right\rangle\left\langle 4S_{1x}S_{2\mu}I_{4\nu}\right| + \left|4S_{1x}I_{3\mu}I_{4\nu}\right\rangle\left\langle 4S_{1x}I_{3\mu}I_{4\nu}\right|\right] \\
&+ \sum_{\mu,\nu,\kappa=x,y,z} \left|8S_{1x}S_{2\mu}I_{3\nu}I_{4\kappa}\right\rangle\left\langle 8S_{1x}S_{2\mu}I_{3\nu}I_{4\kappa}\right|
\end{aligned} \tag{S27}$$

Solving the Liouville–von Neumann equation

The Liouville–von Neumann equation is solved numerically by assuming that the Hamiltonian is time-independent over short time-steps, δt. In this instance, the solution becomes

$$\begin{aligned}
\left|\rho([n+1]\delta t)\right\rangle &= \hat{\hat{P}}(n\delta t)\left|\rho(n\delta t)\right\rangle \\
\hat{\hat{P}}(n\delta t) &= \exp\left[\left(-\mathrm{i}\hat{\hat{H}}(n\delta t) + \hat{\hat{K}} + \hat{\hat{R}}\right)\delta t\right]
\end{aligned} \tag{S28}$$

$\hat{\hat{P}}(n\delta t)$ is the propagator superoperator corresponding to time-step n. When this propagator acts on the density matrix $\left|\rho(t)\right\rangle$, it causes the system to advance one step in time, returning the density matrix $\left|\rho(t+\delta t)\right\rangle$. Starting with an initial density matrix, $\left|\rho(0)\right\rangle$, the system may be propagated to discover the state of the system at an arbitrary time later, $\left|\rho(n\delta t)\right\rangle$.

Initial Condition

The initial density operator, $|\rho(0)\rangle$, is constructed as the statistical mixture of singlet and triplet radical pairs:

$$|\rho(t=0)\rangle = (1-\lambda)\frac{|P_S\rangle}{\langle P_S|P_S\rangle} + \lambda\frac{|P_T\rangle}{\langle P_T|P_T\rangle} \tag{S29}$$

where λ is the initial triplet fraction, and $|P_S\rangle$ and $|P_T\rangle$ are the Liouville-space singlet and triplet projection operators whose Hilbert-space forms are

$$\begin{aligned} |P_S\rangle &\Rightarrow \hat{P}_S = \frac{1}{4}\hat{E} - \hat{S}_1\cdot\hat{S}_2 \\ |P_T\rangle &\Rightarrow \hat{P}_T = \frac{3}{4}\hat{E} + \hat{S}_1\cdot\hat{S}_2 \end{aligned} \tag{S30}$$

Obtaining the results

Experimentally, the observed transient absorption signal is proportional to the total radical concentration. In the simulation, this is calculated as the trace of the density matrix: $I(t) = \mathrm{Tr}(\hat{\rho}(t))$. The results are averaged over a number, N, of equally spaced initial phases, ϕ, of the radiofrequency field and reported as

$$\Delta\Delta A(t) = \varepsilon\sum_{\phi}\frac{1}{N}\left(I_{\text{RF-On}}(\phi,t) - I_{\text{RF-Off}}(\phi,t)\right) \tag{S31}$$

where ε is a scaling factor.

Simulation Parameters

The values used for the parameters described above are listed below. Most are based on experimental observations or were taken from the literature. Least squares fitting was used to determine the relaxation rates and the extinction coefficients.

Molecular Parameters

The *g*-factors used in the simulation are based on literature values.[5] The hyperfine couplings were not found to be sensitive parameters for simulations at B_0 = 1.28 mT because the signal mainly arises from the $F^{\bullet-}$ radical which has no significant hyperfine interactions. Therefore, the hyperfine coupling constants were not fitted. Instead, hyperfine coupling constants of reasonable magnitude were picked such that one was not an integral multiple of the other. The singlet recombination rate was the value as determined in Section 5, above.

g_1 (carotenoid radical)	2.00271
g_2 (fullerene radical)	2.00023
A_3	1.7 mT
A_4	2.5 mT
k_S	1.8×10^7 s^{-1}

Experimental Parameters

Values of the experimental parameters were determined by calibration of the experimental apparatus.

B_0	1.28 mT
B_1	0.14 mT
$\omega_{RF} / 2\pi$	36 MHz
ω_{RF}	2.26×10^8 s^{-1}

Simulation Parameters

As noted above, the assumption is made that the Hamiltonian may be treated as piece-wise constant over a time period δt. The RF cycle was divided into n segments, assuming the B_1 field to be constant within each segment. The random initial phase of the RF field was taken into account by averaging over N values of ϕ. The following values of n, δt and N were found to be sufficient for an accurate simulation.

n	64
$\delta t = 2\pi / n\omega_{RF}$	0.43 ns
N	16

Fitted Parameters

Two fitting parameters were used: the electron relaxation rate, $T^{-1} = T_1^{-1} = T_2^{-1}$, and a scaling factor, ε. These parameters were fitted simultaneously using a least-squares method. Fitting was performed separately for each initial triplet contribution, λ. T^{-1} was the same for both radicals. The scaling factor was used to minimize the difference between the simulation results and the experimental data over the first 1.5 μs of the experiment. The results of the fitting are shown below:

λ	Optimized relaxation rate T^{-1} / 10^6 s^{-1}
0.00	2.40
0.05	2.18
0.07	2.09
0.10	1.96

References

1) H. Hayashi, S. Nagakura, *Bull. Chem. Soc. Jpn.*, 1984, **57,** 322-328.
2) B. van Dijk, J. K. H. Carpenter, A. J. Hoff, P. J. Hore, *J. Phys. Chem. B*, 1998, **102,** 464-472.
3) R. Haberkorn, *Mol. Phys.*, 1976, **32,** 1491-1493.
4) R. R. Ernst, G. Bodenhausen, A. Wokaun, *Principles of Nuclear Magnetic Resonance in One and Two Dimensions*; International Series of Monographs on Chemistry 14; Oxford University Press; New York, 1987.
5) M. Di Valentin, A. Bisol, G. Agostini, M. Fuhs, P. A. Liddell, A. L. Moore, T. A. Moore, D. Gust, D. Carbonera, *J. Am. Chem. Soc.* 2004, **126,** 17074-17086.